Electro-optical properties of excitons in Cu_2O quantum wells. I. Discrete states

David Ziemkiewicz,* Gerard Czajkowski, Karol Karpiński, and Sylwia Zielińska-Raczyńska
Institute of Mathematics and Physics, UTP University of Science and Technology, and Aleje Prof. S. Kaliskiego 7, 85-789 Bydgoszcz, Poland

(Received 27 April 2021; revised 27 June 2021; accepted 12 August 2021; published 25 August 2021)

We present a theoretical calculation of optical functions for Cu_2O quantum well (QW) with Rydberg excitons, in an external homogeneous electric field of an arbitrary strength. Two configurations of an external electric field perpendicular and parallel to the QW plane are considered in the energetic region for discrete excitonic states. With the help of the real density matrix approach, which enables the derivation of the analytical expressions for the QW electro-optical functions, absorption spectra are calculated for the case of the excitation energy below the effective band gap.

DOI: 10.1103/PhysRevB.104.075303

I. INTRODUCTION

Excitons are of a great physical interest since they represent the fundamental optical excitation in semiconductors. In particular in recent years, excitons in Cu_2O have attracted lots of attention [1] due to an experiment, in which the hydrogen-like absorption spectrum of these quasiparticles up to the principal quantum number $n = 25$ has been observed [2]. Since 2014 astonishing properties of these giant Rydberg excitons (RE) have been studied mostly in bulk systems in context of their spectroscopic characteristic as well as their linear and nonlinear interparticle interactions and applications in quantum information technology [3–6]. Most studies of RE in an external electric field are concentrated on the excitation energies below the fundamental gap in Cu_2O [7,8].

The first experiments related to properties of RE focused on natural Cu_2O bulk crystals due to major difficulties in growing high-quality synthetic samples. In the last few years the technological progress enabled the growth of Cu_2O microcrystals with excellent optical material quality and very low point-defect levels [9]. This enabled Cu_2O based low-dimensional systems (quantum wells, wires, and dots) to be realized experimentally [10–13].

Cuprous oxide is a semiconductor characterized by large exciton binding energy and with a significant technological importance in applications such as photovoltaics and solar water splitting. It is also a superior material system for quantum optics that might enable observation of Rydberg excitons in nanostructures. Motivated by technological development and potential applications, investigations of RE in low-dimensional systems have started recently [14–16]. In our previous papers with the help od real density matrix approach (RDMA) we have considered optical properties of RE in quantum dots and quantum wells (QW) [15] and later we have studied Rydberg magnetoexcitons in QW [16]. The applied approach turned out to be useful to describe the fine structure splitting of excitons lines in absorption spectra for any magnetic field strength. The natural step forward at this moment is to study optical response of RE in quantum wells subjected to an interaction with the electric field, for the excitation energy below the effective gap, which results from the modification of the band gap due to the confinement. In such a situation one can distinguish two cases regarding directions of this external electric field, which can be parallel or perpendicular to the quantum well layer. The first case resembles that known from the bulk in an electric field of the energy below the gap [7]; the degenerations of excitonic levels are lifted, an increasing number of peaks appear corresponding to an increasing state number, resonances are shifted and anticrossings of levels are observed. For the electric field perpendicular to the quantum well layer the situation is quite distinct from that in a bulk semiconductor. The electron and the hole creating the exciton are attracted by their Coulomb forces and they are confined in a plane of the quantum well and, as a consequence, large Stark shifts of excitons absorption peaks appear; this phenomenon is called quantum-confined Stark effect (for a recent review see [17]). Bellow we will consider these two cases in details.

The paper is organized as follows. In Sec. II we recall the basic equations of the RDMA, adapted for the case of QWs when an external electric field is applied. Section II is divided into two parts, in which different configurations are considered. First, we consider the case of the electric field applied parallel to the z axis (the growth axis), i.e., perpendicular to the QW planes, and then the case of a lateral electric field is investigated. In both cases we derive analytical expressions for the QW mean effective electro-susceptibility. Those expressions are then used in Sec. III in which detailed calculations for the Cu_2O based QWs are presented. The summary and conclusions of our paper are presented in Sect. IV. The Appendix contains the details of the analytical calculations.

II. THEORY

We consider a Cu_2O quantum well of thickness L, located in the xy plane, with QW surfaces located at $z = \pm L/2$. A linearly polarized electromagnetic wave of the frequency ω incides normally on the QW. The wave vector has only one

*david.ziemkiewicz@utp.edu.pl

component $\mathbf{k} = (0, 0, k_z)$ and the electric field vector $\mathbf{E} = (E_x, 0, 0)$.

We will discuss the changes of the QW optical response when a constant external electric field $\mathbf{F}$ is applied. The polarization of electrons and holes induced by this field leads to a significant decrease of the exciton binding energy. As it was pointed out there are two opposite directions in which one can apply an electric field to QW: an external field is parallel or perpendicular to the layer. In the following subsections both cases will be discussed. As in the previous papers [15,16], we use the real density matrix approach for calculating the QW optical functions (absorption, reflection, and transmission). In particular, the RDMA turned out to be appropriate for computing the effects of external fields since it includes both the relative motion of the carriers and the center-of-mass motion. This approach allows also for including the band mixing effects originating from lifting degenerations of states caused by an external electric field.

A. The electric field parallel to the z axis

We use the RDMA approach, as described in Ref. [16] to determine the electro-optical properties. The RDMA is a mesoscopic approach, which in the lowest order, neglects all effects from the multiband semiconductor structure. However, by the proper estimation of effective masses, this approach include implicitly the influence of admixture of lower valence subband [18]. These effects are included here by using experimental value of effective mass measured in a similar, confined system.

The starting point is the constitutive equation for the so-called coherent amplitude

$$(H_{QW} - \hbar\omega - i\Gamma)Y = \mathbf{ME}, Y \tag{1}$$

with the two-band QW Hamiltonian

$$\begin{aligned} H_{QW} = E_g &+ \frac{1}{2m_e}\left(\mathbf{p}_e - e\frac{\mathbf{r}_e \times \mathbf{B}}{2}\right)^2 \\ &+ \frac{1}{2m_h}\left(\mathbf{p}_h + e\frac{\mathbf{r}_h \times \mathbf{B}}{2}\right)^2 + e\mathbf{F}\cdot(\mathbf{r}_e - \mathbf{r}_h) \\ &+ V_{\text{conf}}(\mathbf{r}_e, \mathbf{r}_h) - \frac{e^2}{4\pi\epsilon_0\epsilon_b|\mathbf{r}_e - \mathbf{r}_h|}, \end{aligned}$$

where $\mathbf{B}$ is the magnetic field vector, $\mathbf{F}$ the electric field vector, V_{conf} denotes the surface potential for electrons and holes, m_h, m_e are the hole and the electron effective masses. We separate the exciton center-of-mass and relative motion, and consider the case of $\mathbf{B} = 0$, for $\mathbf{F} \parallel \hat{\mathbf{z}}$ and the dipole density $\mathbf{M} \parallel \mathbf{E}$. The electron-hole interaction is used in the two-dimensional approximation, which enables one to obtain the solutions in an analytical form. Since we are particularly interested in the problem of the electric field's influence on the higher excitonic levels, we propose to use the two-dimensional approximation. For p excitons the spatial extension of the excitonic wave function increases approximately as their square number j^2 and their extension for higher states can be much larger than the quantum well thickness. Moreover the energy values for higher excitonic states differ only slightly from these of three-dimensional system and the difference between two- and three-dimensional calculations affects mostly the oscillator strengths. In particular, the energy of the confined state is higher by less than 10% for $j > 10$.

The calculations of electro-optical properties become much simpler when we consider a quantum well with a parabolic confinement potential in the form of a harmonic oscillator potential $V_{\text{conf}} = \frac{1}{2}m_e\omega_{ez}^2 z_e^2 + \frac{1}{2}m_h\omega_{hz}^2 z_h^2$, where the energies $\hbar\omega_{ez}$, $\hbar\omega_{hz}$ correspond to the electron and hole barriers. For the considered geometry the QW Hamiltonian has the form

$$\begin{aligned} H_{\text{QW}} = E_g &+ H^{(1D)}_{m_{ez},\omega_{ez}}(\zeta_e) + H^{(1D)}_{m_h,\omega_{hz}}(\zeta_h) \\ &+ H^{(2D)}_{\text{Coul}}(\boldsymbol{\rho}) - \frac{(eF)^2}{2m_e\omega_{ez}^2} - \frac{(eF)^2}{2m_h\omega_{hz}^2}, \end{aligned} \tag{2}$$

and contains the one-dimensional oscillator Hamiltonian

$$H^{(1D)}_{m,\omega}(z) = \frac{p_z^2}{2m} + \frac{1}{2}m\omega^2 z^2, \tag{3}$$

and the two-dimensional Coulomb Hamiltonian

$$H^{(2D)}_{\text{Coul}}(\boldsymbol{\rho}) = \frac{\mathbf{p}_\parallel^2}{2\mu} - \frac{e^2}{4\pi\epsilon_0\epsilon_b\rho}, \tag{4}$$

where $\zeta_e = z_e + z_{0e}$, $z_{0e} = eF/m_e\omega_{ez}^2$. The two-dimensional potential allows for analytical calculations including arbitrary high exciton states, which is the key point for Rydberg excitons, whereas more accurate calculations (for example, variational) can be performed only for the lowest or few lower excitonic states.

Using the long wave approximation we seek the solutions of Eq. (1) in the form

$$\begin{aligned} Y(\rho, \zeta_e, \zeta_h) = E(Z) &\sum_{jmN_eN_h} c_{jmN_eN_h}\psi_{jm}(\boldsymbol{\rho})\psi^{(1D)}_{\alpha_e,N_e}(\zeta_e) \\ &\times \psi^{(1D)}_{\alpha_h,N_h}(\zeta_h), \end{aligned} \tag{5}$$

where ψ_{jm} are the normalized eigenfunctions of the two-dimensional Coulomb Hamiltonian,

$$\begin{aligned} \psi_{jm}(\rho, \phi) &= R_{jm}(\rho)\frac{e^{im\phi}}{\sqrt{2\pi}}, \\ R_{jm} &= A_{jm}e^{-2\lambda\rho}(4\lambda\rho)^{|m|}L_j^{|2m|}(4\lambda\rho), \\ \lambda &= \frac{1}{1 + 2(j + |m|)}, \\ A_{jm} &= \frac{4}{(2j + 2|m| + 1)^{3/2}}\left[\frac{j!}{(j + 2|m|)!}\right]^{1/2}, \end{aligned} \tag{6}$$

and $L_n^\alpha(x)$ are the Laguerre polynomials. The $\rho = r/a^*$ is the scaled space variable and $\psi^{(1D)}_{\alpha,N}(z)$ $(N = 0, 1, \ldots)$ are the quantum oscillator eigenfunctions of the Hamiltonian (3).

Here we use the transition dipole density in the form [16]

$$M(\boldsymbol{\rho}, z_e, z_h) = \frac{M_0}{2\rho_0^3}\rho\, e^{-\rho/\rho_0}\frac{e^{i\phi}}{\sqrt{2\pi}}\delta(z_e - z_h). \tag{7}$$

M_0 is the integrated strength, the coherence radius is defined as $\rho_0 = r_0/a^*$, with $r_0 = \sqrt{\frac{\hbar^2}{2\mu E_g}}$ and a^* is the excitonic

Bohr radius. These coefficients are connected through the longitudinal-transversal energy Δ_{LT}

$$(M_0\rho_0)^2 = \frac{4}{3}\frac{\hbar^2}{2\mu}\epsilon_0\epsilon_b a^* \frac{\Delta_{LT}}{R^*}\, e^{-4\rho_0}. \tag{8}$$

Assuming that the electromagnetic wave of the component $E(Z)$ is linearly polarized, we substitute Y from Eq. (5) into Eq. (1) to calculate the expansion coefficients $c_{jmN_eN_h}$

$$c_{j1N_eN_h} = \langle \Psi_{N_eN_h}\rangle_\infty b_{j1}\Bigg[E_g - \hbar\omega - i\Gamma + W_{N_e} + W_{N_h} - \frac{(eF)^2}{2m_{ez}\omega_{ez}^2} - \frac{(eF)^2}{2m_{hz}\omega_{hz}^2}\Bigg]^{-1},$$

with the following definitions

$$\begin{aligned}
\langle \Psi_{N_eN_h}\rangle_\infty &= \int_{-\infty}^{\infty} \psi^{(1D)}_{\alpha_e,N_e}(\zeta_e)\psi^{(1D)}_{\alpha_h,N_h}(\zeta_h)dz \\
&= \sqrt{\frac{\alpha_e\alpha_h}{\pi\, 2^{N_e+N_h}N_e!\, N_h!}} \\
&\quad\times \int_{-\infty}^{\infty} dz\Bigg\{ H_{N_e}[\alpha_e(z+z_{0e})]e^{-\frac{\alpha_e^2(z+z_{0e})^2}{2}} \\
&\quad\times H_{N_h}[\alpha_h(z-z_{0h})]e^{-\frac{\alpha_h^2(z-z_{0h})^2}{2}}\Bigg\}, \qquad (9)\\
W_{N_e} &= \left(N_e+\frac{1}{2}\right)\hbar\omega_{ez}, \\
W_{N_h} &= \left(N_h+\frac{1}{2}\right)\hbar\omega_{hz}, \\
b_{j1} &= \frac{2\mu}{\hbar^2}\Bigg\{(M_0\rho_0)\frac{6}{\sqrt{2}} \\
&\quad\times\sqrt{\frac{(j+1)(j+2)}{(j+3/2)^5}}(1+2\rho_0\lambda_{j1})^{-4}F\left(-j,4;3;\frac{1}{s}\right)\Bigg\} \\
s &= \frac{1+2\rho_0\lambda_{j1}}{4\rho_0\lambda_{j1}}, \\
\lambda_{j1} &= \frac{1}{2j+3}, \qquad (10)
\end{aligned}$$

and $F(\alpha,\beta;\gamma;z)$ denotes a hypergeometric series [19] (in Ref. [16] the calculation of b_{j1} is extensively presented). The quantities W_{N_e}, W_{N_h} are eigenvalues of the Hamiltonian (3). In the RDMA the total polarization of the medium is related to the coherent amplitude Y by

$$\mathbf{P}(\mathbf{R}) = 2\mathrm{Re}\int d^3r\, \mathbf{M}(\mathbf{r})Y(\mathbf{R},\mathbf{r}) \tag{11}$$

where $\mathbf{R}$ is the electron-hole pair center-of-mass coordinate. This, in turn, is used in the Maxwell's equation

$$c^2\nabla^2\mathbf{E}(\mathbf{R}) - \epsilon_b\ddot{\mathbf{E}} = \frac{1}{\epsilon_0}\ddot{\mathbf{P}}(\mathbf{R}). \tag{12}$$

Using the long wave approximation we obtain the coherent amplitude Y from Eq. (1) as linearly dependent on the electric field $\mathbf{E}$. Then, from Eq. (11), one can determine the susceptibility $\chi(\mathbf{R})$ [16].

For linearly polarized wave, in the considered configuration for the wave propagating in the z direction, we consider one component $E(Z)$ and one $P(Z)$ of the electric and polarization vectors, obtaining the position-dependent susceptibility $\chi(Z) = \frac{P(Z)}{\epsilon_0 E(Z)}$. Below we will use the mean effective QW susceptibility,

$$\chi = \frac{1}{L}\int_{-L/2}^{L/2}\frac{P(Z)}{\epsilon_0 E(Z)}\,dZ. \tag{13}$$

For the considered case of the electric field perpendicular to the QW layer, the polarization determined from Eq. (11), regarding also the form of $\mathbf{M}$, can be written in the form

$$P(Z) = 2M_0\sum_{N_e=0}^{^Ne\,\max}\sum_{N_h=0}^{^Nh\,\max}\sum_{j=0}^{J}\Big\{c_{j1N_eN_h}b_{j1} \times \psi^{(1D)}_{\alpha_e,N_e}(Z+z_{e0})\psi^{(1D)}_{\alpha_h,N_h}(Z-z_{h0})\Big\}.$$

Here J denotes the upper limit of j, which corresponds to the number of excitonic states taken into account. Using Eq. (13) we arrive at the equation determining the mean effective susceptibility for a QW, when the homogeneous electric field F is applied perpendicular to the QW plane,

$$\chi^{(2D)}(\omega) = 48\epsilon_b\frac{\Delta_{LT}}{R^*}\left(\frac{a^*}{L}\right)\sum_{N_e=0}^{^Ne\,\max}\sum_{N_h=0}^{^Nh\,\max}\sum_{j=0}^{J}\frac{f_j^{(2D)}\langle\Psi_{N_eN_h}\rangle_\infty\langle\Psi_{N_eN_h}\rangle_L}{L(E_g-\hbar\omega+E_{j1}+W_{N_e}+W_{N_h}+\Delta E-i\Gamma_{jN_eN_h})}, \tag{14}$$

where

$$\begin{aligned}
f_{j1}^{(2D)} &= 48\frac{(j+1)(j+2)}{\left(j+\frac{3}{2}\right)^5}\frac{\left[F\left(-j,4;3;\frac{4\lambda_{j1}\rho_0}{1+2\lambda_{j1}\rho_0}\right)\right]^2}{(1+2\lambda_{j1}\rho_0)^8}, \\
E_{jm} &= -\frac{4}{(2j+2|m|+1)^2}R^*, \\
\langle\Psi_{N_eN_h}\rangle_L &= \\
&= \sqrt{\frac{\alpha_e\alpha_h}{\pi\, 2^{N_e}N_e!\, 2^{N_h}N_h!}}\int_{-L/2}^{L/2}dz\left\{H_{N_e}(z+z_{0e})e^{-\alpha_e^2(z+z_{0e})^2/2}\,H_{N_h}(z-z_{0h})e^{-\alpha_h^2(z-z_{0h})^2/2}\right\}, \qquad (15)
\end{aligned}$$

The Stark shift is given by

$$\Delta E = -\frac{e^2F^2}{2m_{ez}\omega_{ez}^2} - \frac{e^2F^2}{2m_{hz}\omega_{hz}^2}. \tag{16}$$

For further calculations we have to specify the confinement parameters α_{e,α_h}.

We identify the oscillator energies $W_{N_e=0}, W_{N_h=0}$ with those of the lowest energies of the infinite well potentials

$$W_{N_e=0} = \frac{\hbar^2}{2m_e}\frac{\pi^2}{L^2}, \quad W_{N_h=0} = \frac{\hbar^2}{2m_h}\frac{\pi^2}{L^2}, \tag{17}$$

so the coefficients have the form

$$\alpha_e = \alpha_h = \alpha = \frac{1}{a^*}\left(\frac{\pi}{L}\right). \tag{18}$$

For such confinement parameters the derivation of the specific form of $\langle\Psi_{N_eN_h}\rangle_\infty$ and $\langle\Psi_{N_eN_h}\rangle_L$ for the lowest combinations of the quantum numbers N_e, N_h is presented in the Appendix. The Stark shift (16) expressed by the confinement parameters depends also on the total excitonic mass and the applied field strength $f = \frac{F}{F_I}$ ($F_I = \frac{R^*}{ea^*}$ is the ionization field):

$$\Delta E = -\frac{1}{4\pi^4} f^2 \left(\frac{M_{\rm tot}}{\mu}\right)\left(\frac{L}{a^*}\right)^4 R^*. \tag{19}$$

As mentioned before, the energies E_{jm} approach the bulk relation $\sim 1/j^2$ in the limit of large j. For Cu_2O the ionization field is quite large (due to the small size of the excitonic Bohr radius), so realistic experimental situations correspond to $f \ll 1$. Such range of the field strengths is discussed in our paper. As follows from Eq. (14), the applied electric field in this configuration causes the appearance of confinement states with $N_e \neq N_h$, which, in the model with equal confinement parameters for electron and hole, are absent in the case without the field. As an illustration, we present the formula for the mean effective electro-susceptibility, where the lowest confinement states ($N_e = N_h = 0$), ($N_e = 1, N_h = 0$), ($N_e = 0, N_h = 1$), and J 2D exciton states are accounted for:

$$\begin{aligned}\chi^{(2D)}(\omega) = &\sum_{j=0}^{J} \frac{\epsilon_b \Delta_{LT} a^* f_j^{(2D)} \langle\Psi_{00}\rangle_\infty \langle\Psi_{00}\rangle_L}{L(E_g - \hbar\omega + E_{j1} + W_{N_e=0} + W_{N_h=0} + \Delta E - i\Gamma_{j00})} \\ &+ \sum_{j=0}^{J} \frac{\epsilon_b \Delta_{LT} a^* f_j^{(2D)} \langle\Psi_{10}\rangle_\infty \langle\Psi_{10}\rangle_L}{L(E_g - \hbar\omega + E_{j1} + W_{N_e=1} + W_{N_h=0} + \Delta E - i\Gamma_{j10})} \\ &+ \sum_{j=0}^{J} \frac{\epsilon_b \Delta_{LT} a^* f_j^{(2D)} \langle\Psi_{01}\rangle_\infty \langle\Psi_{01}\rangle_L}{L(E_g - \hbar\omega + E_{j1} + W_{N_e=0} + W_{N_h=1} + \Delta E - i\Gamma_{j01})}.\end{aligned} \tag{20}$$

The expressions for the quantities $\langle\Psi_{00}\rangle_\infty \langle\Psi_{00}\rangle_L$, $\langle\Psi_{10}\rangle_\infty \langle\Psi_{10}\rangle_L$, and $\langle\Psi_{01}\rangle_\infty \langle\Psi_{01}\rangle_L$ are given in the Appendix. All relevant parameters are summarized in the Table I. Note that the masses are taken from experimental results [20], which are consistent with experimental values from Ref. [14], where similar, highly-confined system is investigated. These values include the contribution from admixture of Γ_8 subband.

TABLE I. Band parameter values for Cu_2O, Rydberg energy and excitonic radius calculated from effective masses; masses in free electron mass m_0, the ionization field $F_I = R^*/(ea^*)$

Parameter	Value	Unit	Reference
E_g	2172.08	meV	[15]
R^*	87.78	meV	[15]
Δ_{LT}	1.25×10^{-3}	meV	[15]
Γ	$3.88/(j+1)^3$	meV	[5]
m_e	1.0	m_0	[14,19]
m_h	0.7	m_0	[14,19]
$M_{\rm tot}$	1.56	m_0	[15]
μ	0.363	m_0	[15]
a^*	1.1	nm	[15]
r_0	0.22	nm	[15]
ϵ_b	7.5		[15]
F_I	1.02×10^3	kV/cm	

B. The electric field parallel to *x* axis

In this section we will discuss the case of the electric field **F** parallel to the layer and still we will consider the case of the excitation energy $\hbar\omega$ smaller than the effective band gap. The electric field can be considered as a perturbation and methods can be used similar to those used in our previous papers for the electric field applied to bulk crystal [7] or for the magnetoexcitons in a QW [16] can be used. We use confinement parabolic e-h potential and the two-dimensional Coulomb interaction the QW Hamiltonian, which consists of the following operators:

$$\begin{aligned}H_{\rm QW} = &E_g + H^{(1D)}_{m_e,\omega_{ez}}(z_e) + H^{(1D)}_{m_h,\omega_{hz}}(z_h) \\ &+ H^{(2D)}_{\rm Coul}(\boldsymbol{\rho}) + eF(x_e - x_h).\end{aligned} \tag{21}$$

Considering the term $eF(x_e - x_h)$ as a perturbation, we seek the solution of the constitutive equation (1) in terms of the eigenfunctions of the unperturbed part of the Hamiltonian (21),

$$Y = \sum_{jmN_eN_h} c_{jmN_eN_h} \psi^{(2D)}_{jm}(\rho,\phi)\psi^{(1D)}_{\alpha_e,N_e}(z_e)\psi^{(1D)}_{\alpha_h,N_h}(z_h). \tag{22}$$

The functions are defined in the previous section. Proceeding in a similar way as it was done in subsection A, i.e., substituting the expansion (22) into the constitutive equation (1) with the Hamiltonian (21) and the dipole density (7), we arrive to a

set of equations for the expansion coefficients:

$$\sum_{j=0}^{J-1}\sum_{N_eN_h} c_{j1N_eN_h}\kappa^2_{j1N_eN_h}\delta_{ij}\delta_{N_eN_h} + \sum_{j=0}^{J-1}\sum_{N_eN_h} c_{j0N_eN_h}V^{10}_{ij}\delta_{N_eN_h} + \sum_{j=0}^{J-1}\sum_{N_eN_h} c_{j2N_eN_h}V^{12}_{ij}\delta_{N_eN_h} = \frac{2\mu}{\hbar^2}\frac{1}{a^*}\langle R_{i1}|M\rangle\langle\Psi_{N_eN_h}\rangle_\infty,$$
$$i = 0, 1, \ldots, J-1, \tag{23}$$

and

$$\sum_{j=0}^{J-1}\sum_{N_eN_h} c_{j0N_eN_h}\kappa^2_{j0N_eN_h}\delta_{ij}\delta_{N_eN_h} + 2\sum_{j=0}^{J-1}\sum_{N_eN_h} c_{j1N_eN_h}V^{01}_{ij}\delta_{N_eN_h} = b_i;$$
$$i = J, J+1, \ldots$$
$$\sum_{j=0}^{J-1}\sum_{N_eN_h} c_{j2N_eN_h}\kappa^2_{j2N_eN_h}\delta_{ij}\delta_{N_eN_h} + 2\sum_{j=0}^{J-1}\sum_{N_eN_h} c_{j1N_eN_h}V^{21}_{ij}\delta_{N_eN_h} = b_i;$$
$$i = 2J, 2J+1, \ldots$$

where the following definitions were used:

$$\kappa^2_{jmN_eN_h^2} = \frac{1}{R^*}(E_g - \hbar\omega + E_{jm} + W_{N_e} + W_{N_h} - i\Gamma). \tag{24}$$

V are the matrix elements

$$V^{01}_{\ell s} = \frac{1}{2}f\int_0^\infty \rho^2\, d\rho\, R_{\ell 0}(\rho)R_{s1}(\rho),$$
$$V^{10}_{\ell s} = \frac{1}{2}f\int_0^\infty \rho^2\, d\rho\, R_{\ell 1}(\rho)R_{s0}(\rho), \tag{25}$$
$$\ell, s = 0, 1, \ldots, J-1,$$
$$V^{12}_{\ell s} = \frac{1}{2}f\int_0^\infty \rho^2\, d\rho\, R_{\ell 1}(\rho)R_{s2}(\rho).$$

The Eqs. (23) form the set of $3J$ linear algebraic equations. They can be put into a matrix form

$$\underline{\underline{A}}\mathbf{X} = \mathbf{b},$$
$$\mathbf{X} = (x_1, x_2, \cdots x_{3J}), \tag{26}$$
$$\mathbf{b} = (b_1, b_2, \cdots b_{3J}).$$

The matrix elements $\underline{\underline{A}}$ and the components of the vector $\mathbf{b}$ are defined in [21], where the derivation is presented step by step. With the solutions $\mathbf{X}$ one can obtain the expression for the effective QW electro-susceptibility for $F \parallel \hat{\mathbf{x}}$,

$$\chi^{(2D)}(\omega) = 48\epsilon_b\frac{\Delta_{LT}}{R^*}\left(\frac{a^*}{L}\right)\mathrm{erf}\left(\frac{L\sqrt{p}}{2}\right)\frac{\alpha_e\alpha_h}{p}\sum_{i=1}^{J} b_i\, x_i. \tag{27}$$

By considering only $j = 1$ exciton, the energy shifts of s, p, d levels ($m = 0, 1, 2$, respectively) are described by a third-degree polynomials [21] and in general are proportional to f^2. The energy shifts may differ by sign, so that anticrossings may occur. When the field strength f increases, for a certain critical value of f the inversion of places appears: the level p will be situated above the level d (in energetic scale).

III. RESULTS AND DISCUSSION

A. The F field perpendicular to the QW layer (F||ẑ)

The behavior of electro-absorption for the electric field perpendicular to quantum well layers is quite distinct from that in bulk semiconductors, which is a straightforward consequence of the quantum well gist. Vividly speaking, an electric field perpendicular to the layer pulls the hole and electron (forming the exciton) in opposite directions squashing them against the walls of quantum well and both particles are strongly attracted by their Coulomb interaction. Taking into account higher excitonic states one can observe that the exciton absorption peaks are broadened and, as a consequence of constrains due to QW, there appear large Stark shifts (towards lower energies), which is known as the quantum-confined Stark effect.

Figure 1 shows the imaginary part of susceptibility calculated from Eq. (20) for $L = 10$ nm and a range of values of electric field. There is a complicated pattern of absorption lines corresponding to various excitonic states $j = 0, 1, 2...$ and confinement states $N_e = 0, 1, 2...$ $N_h = 0, 1, 2....$ The excitonic number j has a noticeable impact on linewidth. All resonances experience an energy red-shift proportional to f^2. One can observe that some states are visible only in some range of values of f. In general, lines with higher confinement state numbers are characterized by higher energy and lower amplitude. To identify the particular states, the numbers (j, N_e, N_h) are shown on Fig. 2. The identification of states becomes very complicated, due to a large number of overlapping peaks, which is also the case in the bulk crystal [22], but here it turned out to be possible to some extend, i.e., for $j = 0, 1$, to assign quantum numbers to the resonances. The oscillator strength of the basic excitonic states (0,0,0), (1,0,0) etc., decreases with f. For example, $j = 1$ exciton (∼2165 meV, marked [1,0,0]) and $j = 2$ exciton (∼2175 meV) disappear around $f = 0.05$ and $f = 0.01$, which corresponds to 51 kV/cm, and 10 kV/cm. The latter

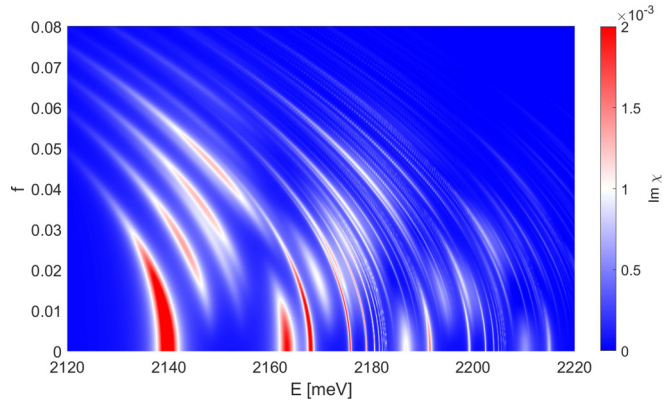

FIG. 1. Imaginary part of susceptibility as a function of energy and electric field f for $L = 10$ nm.

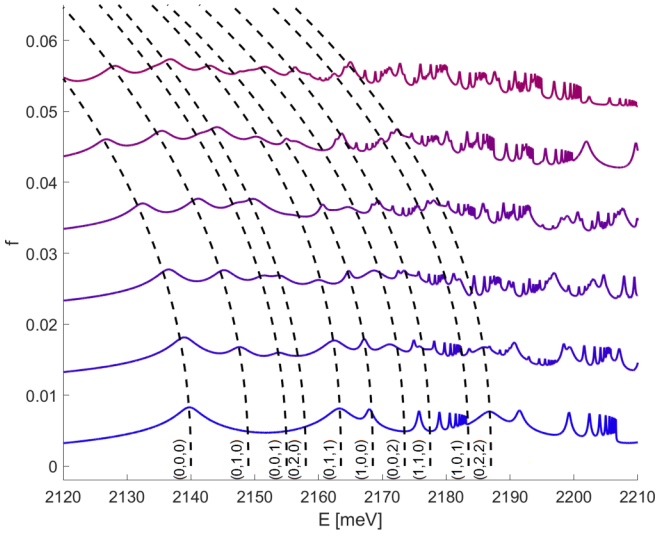

FIG. 2. The same as Fig. 1, shown for a few selected values of f. Selected lines are marked with dashed lines and identified.

value can be compared with the results presented in [23] and is consistent with them. Overall, the upper limit of the considered field values is slightly larger than in the available experimental data [8,23].

The first line (0,0,0) is a starting point of several series with increasing j, N_e, N_h. The excitonic states j approach asymptotically a value of $E_g' \approx 2190$ meV, which is the gap energy with an additional shift due to the confinement energy. The increase of N_e corresponds to the change of energy $\Delta E \sim 8.5$ meV [for example, energy distance between the states (0,0,0) and (0,1,0)]; the gap between consecutive N_h lines [(0,0,0) and (0,0,1)] is roughly $\Delta E \approx 15$ meV. Again, one can see that some lines are visible only in some range of f; for example, the state (0,1,1) disappears around $f \approx 0.035$. The lines corresponding to high values of j, N_e, N_h extend beyond the band gap, creating a very complicated pattern in this region, especially for large values of f.

To further explore the impact of confinement quantum numbers on the positions of resonances, the susceptibility has been calculated taking into account only $j = 0$ excitonic state. The results are shown on the Fig. 3. Four different cases are presented where either N_e or N_h is set to 0 or 1. Fig. 3(a) shows the spectrum for $N_e = 0$. One can see that the lines corresponding to $N_h = 1, 2, 3, 4$ are equally spaced and exhibit the same energy shift with f. Higher values of N_h correspond to weaker lines with a higher minimal value of f above which the line becomes visible. The only line present at $f = 0$ is $N_e = N_h = 0$. The spectrum becomes slightly more complex when $N_e = 1$, as shown on Fig. 3(b); with the exception of $N_h = 0$, the lines split into two ranges of f where they have nonzero amplitude. Again, the amplitude decreases with N_h while the energy increases with N_h in a linear manner. Fig. 3(c) is very similar to Fig. 3(a), with main difference being smaller energy spacing between $N_e = 1, 2, 3, 4$ lines. In the same manner, Fig. 3(d) has the same structure as Fig. 3(b). One can see that only $N_e = N_h$ states are visible for $f = 0$. This is also visible in Fig. 2.

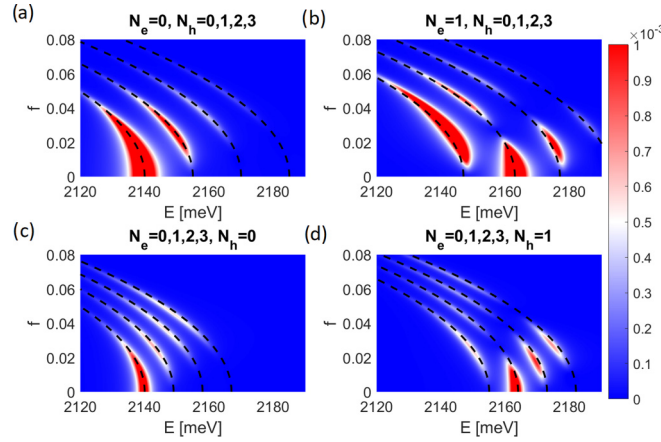

FIG. 3. Imaginary part of susceptibility calculated for $L = 10$ nm, $j = 0$ and (a) $N_e = 0$, (b) $N_e = 1$, (c) $N_h = 0$, and (d) $N_h = 1$.

The above discussed line series are repeated for every value of excitonic state number j. Figure 4(a) shows the spectrum calculated for $j = 0, 1, ..., 9$ and $N_e = N_h = 0$. One can see a typical excitonic line series with energy asymptotically approaching some constant value. With an increase of either N_e [Fig. 4(b)] or N_h [Fig. 4(c)], the whole spectrum is shifted in energy and the range of values of f where the lines are visible moves up. Finally, Fig. 4(d) shows the case of various values of $N_e = N_h = 1, 2, 3, 4$; one can observe that every consecutive line splits into more separate parts. By observing higher confinement states, we can conclude that for any combination of N_e, N_h, the line splits into $\min(N_e, N_h) + 1$ areas where its amplitude is nonzero. Figure 5 shows the dependence on L for the same confinement state combinations as in Fig. 3. One can see that in all cases, the energy diverges as $L \to 0$; however, in contrast to the electric field dependence, the speed of divergence and the exact location of the asymptote is different for various values of N_e, N_h. For example, on Fig. 5(a) the line $N_h = 0$ approaches infinity as $L \to 2$ nm, while $N_h = 3$ diverges at $L \to 6$ nm. One can also see that the lines corresponding to higher N_h are present in

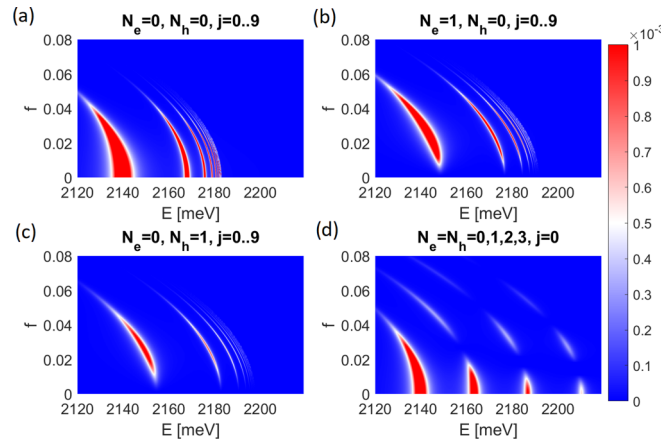

FIG. 4. Imaginary part of susceptibility calculated for $L = 10$ nm, $j = 0..9$ and (a) $N_e = N_h = 0$, (b) $N_e = 1$, (c) $N_h = 1$, and (d) $j = 0$, $N_e = N_h = 1, 2, 3, 4$.

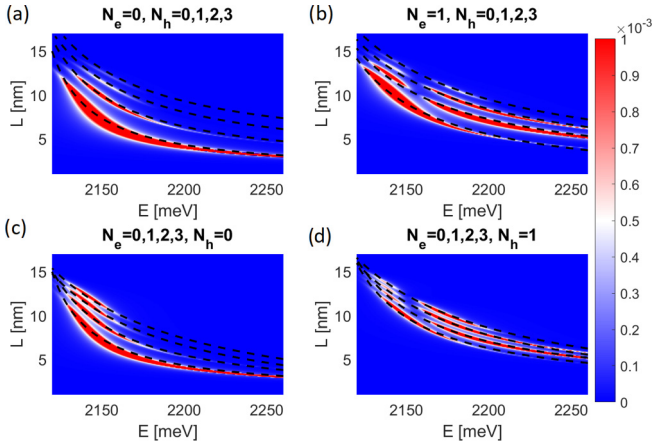

FIG. 5. Imaginary part of susceptibility calculated for $L = 10$ nm, $j = 0$ and (a) $N_e = 0$, (b) $N_e = 1$, (c) $N_h = 0$, and (d) $N_h = 1$.

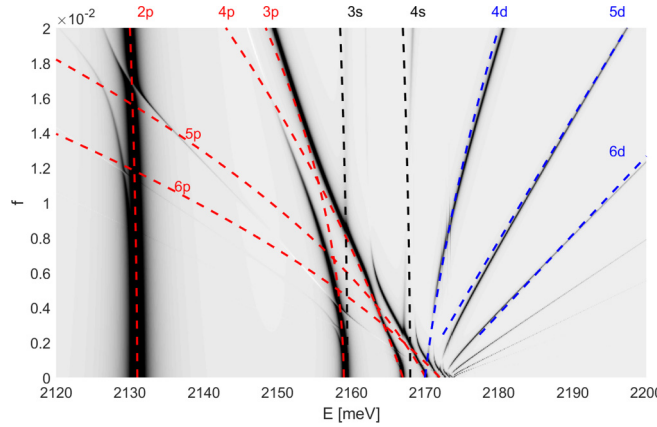

FIG. 7. Imaginary part of susceptibility (brightness, in log scale) as a function of energy and electric field f.

a narrower range of values of L. The spectrum for $N_e = 1$ [Fig. 5(b)] exhibits the same splitting into two ranges of L as in the case of electric field dependence. The minimum thickness for which those lines appear is slightly higher than for $N_e = 0$. Again, Figs. 5(c) and 5(d) are analogous to Figs. 5(a) and 5(b), but with smaller energy spacing between lines.

B. The F field parallel to the QW layer (F||$\hat{x}$)

For the case of the electric field parallel to the layer we deal with the effects that are qualitatively similar to those known from the bulk semiconductor. The main observations are lifting degeneracy of excitonic spectrum due to the external field and appearance of avoided crossings.

Figure 6 presents the absorption spectrum calculated from Eq. (27) for selected values of electric field f and QW thickness $L = 20$ nm. At $f = 0$, a standard series of p-exciton lines is visible. One can that the exciton energies approach $E \approx 2175$ meV, which is larger than E_g due to the L-dependent energy shift. The state $2p$ exhibits a very tiny shift with changing the electric field, but the effect is much stronger for higher states $3p$, $4p$ etc. Due to the fact that

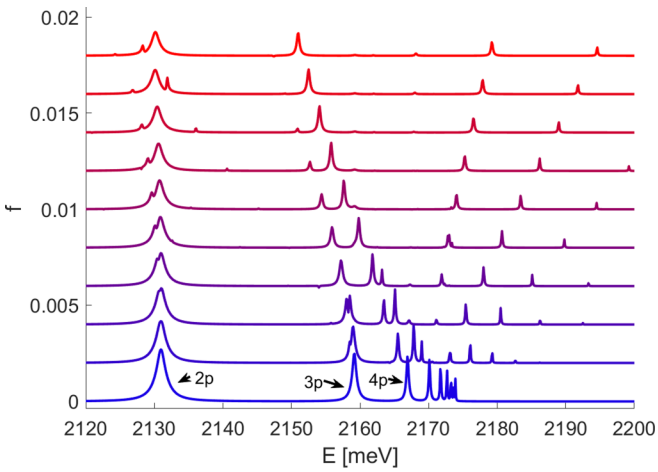

FIG. 6. Imaginary part of susceptibility as a function of energy and electric field f.

the state energy decreases with f and the reduction is faster for upper states, a lot of lines overlaps and anticrossing are observed. In the high-energy region, multiple small peaks are visible; these maxima correspond to the d excitons, starting from $3d$ state. Finally, one can observe that the absorption amplitude decreases slowly with the electric field. To better understand the structure of the spectrum, a continuous range of values of f is investigated on Fig. 7. The s, p, and d excitons are marked by black, red and blue lines, accordingly. The p excitons exhibit an approximately quadratic energy shift with f; due to the line overlap, only $2p$ and $3p$ excitonic lines are clearly visible in the full range of f. One can observe a significant anticrossing of $3p$ and $4p$ lines originating from nondiagonal matrix elements in Eq. (26). Interestingly, while the s exciton lines are not distinctly visible, they also cause anticrossings (for example, intersection of $4s$ and $5p$ lines at $f = 4 \times 10^{-3}$). The d exciton lines appear at some minimal value of $f \sim 2 \times 10^{-3}$ and are linearly upshifted with f.

A more detailed analysis of single excitonic state $j = 2$ is shown on Fig. 8. The overall spectrum structure follows the one presented in [24]; the strongest $3p$ line (red) starts from $E \approx 2157$ meV and exhibits quadratic energy shift. There is a pair of $3d$ lines, which originate from a point $E \approx 2165$ meV and split in a linear manner with f. These lines become visible at $f \sim 2 \times 10^{-}3$; in a high field regime, their amplitude becomes comparable to the p state. Another feature of the spectrum is a d exciton triplet. Those lines are visible mostly in the region of their anticrossing with p and s state. The $3s$ state is also visible for sufficiently strong field; its energy is almost independent of f. Note that while for $f = 0$ the s exciton has lower energy than p exciton, the situation reverses for high field due to the fact that the s state very weakly affected by the external field in contrast to the p and d states. Such a phenomenon was observed experimentally by Agekyan [24].

Even more complicated spectrum is obtained for $n = 5$ state (Fig. 9). In addition to single p, single s, and two d states, there are multiple lines that can be attributed to anticrossings with $4d$ and $6d$ excitons. For any given n, the states form a structure close to the standard Stark fan [8] and its width is comparable with experimental results in Ref. [8] for the same electric field value. Again, due to the field-induced downshift, the $5p$ state line crosses the lines of $3s$, $4s$, and $5s$ excitons;

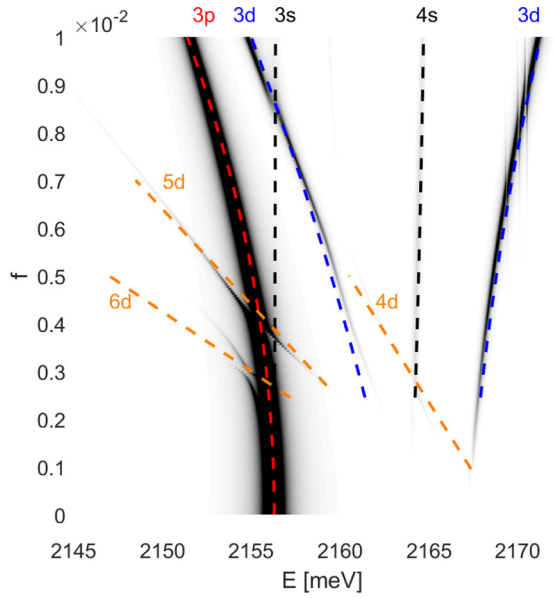

FIG. 8. Imaginary part of susceptibility (brightness, in log scale) near the $3p$ excitonic state as a function of energy and electric field f.

due to the lower linewidth of $5p$ level, these anticrossings are more apparent. Finally, Fig. 10 shows the dependence of exciton energy on the QW thickness L, calculated for electric field $f = 0.01$. The shift dependence of the lower states is more pronounced for wider quantum wells. Moreover, one can see two series of states: the p excitons and the high-energy d excitons. Both types of states exhibit a strong upshift with decreasing L, approaching $E \to \infty$ in the very thin quantum well limit of $L \to 3$ nm.

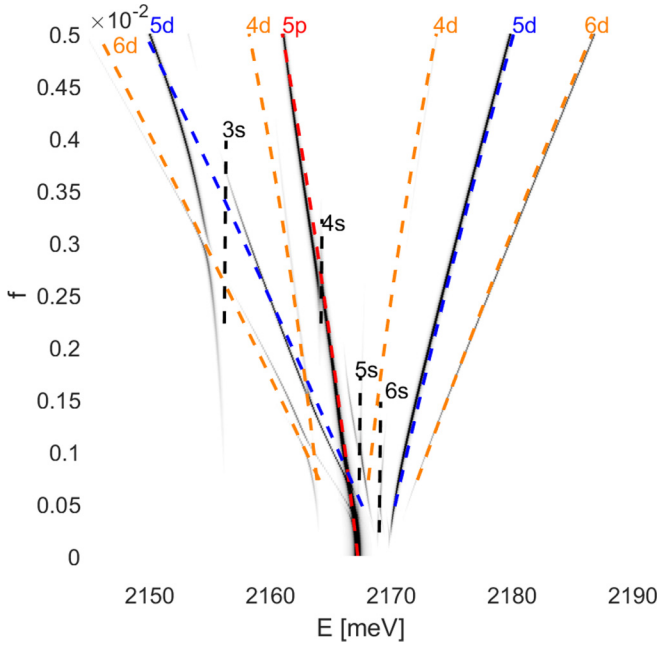

FIG. 9. Imaginary part of susceptibility (brightness, in log scale) near the $5p$ excitonic state as a function of energy and electric field f.

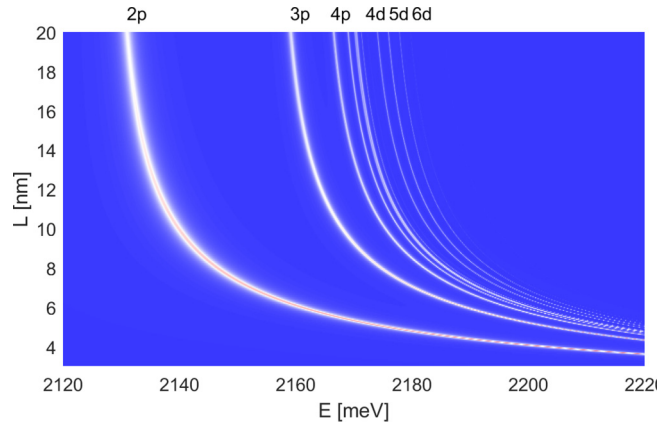

FIG. 10. Imaginary part of susceptibility (color) as a function of energy and well thickness L.

IV. CONCLUSIONS

In this paper we have studied the electro-optical properties of Cu_2O QWs with Rydberg excitons for two different orientations of the applied external electric field, for excitation energies below the effective gap. For the electric field applied in the z direction, and in the considered field strengths range, the quadratic Stark red shift of resonance energies prevails, depending on the QW thickness and the total exciton mass. New resonances appear, which are not allowed, for symmetry reasons, when the electric field is absent. We observe even more complicated dependencies in the case of the lateral applied field. The resonances can be both red- and blue shifted. We observe a considerable interlevel mixing and splitting caused by differences in energy shifts and various excitonic states due to the interplay between the confinement and the electric field. We believe that tunability of optical properties of QW with RE, which is enabled in both electric field configurations makes them suitable for applications as flexible devices in nanotechnology.

APPENDIX: QUANTITIES $\langle\Psi_{N_eN_h}\rangle_\infty$, $\langle\Psi_{N_eN_h}\rangle_L$

We use the definitions (9) and (15) to calculate the quantities $\langle\Psi_{NeN_h}\rangle_\infty$, and $\langle\Psi_{NeN_h}\rangle_L$. We take three combinations: $N_e = 0, N_h = 0$, $N_e = 1, N_h = 0$, and $N_e = 0, N_h = 1$. Inserting the definitions of the Hermite polynomials H_0, H_1, and performing the respective integrations, one obtains

$$\langle\Psi_{00}\rangle_\infty = \sqrt{\frac{\alpha_e\alpha_h}{p}}\exp\left[-\frac{\alpha_e^2\alpha_h^2(z_{0e}+z_{0h})^2}{2(\alpha_e^2+\alpha_h^2)}\right], \quad \text{(A1)}$$

$$\langle\Psi_{00}\rangle_L = \sqrt{\frac{\alpha_e\alpha_h}{p}}\exp\left[-\frac{\alpha_e^2\alpha_h^2(z_{0e}+z_{0h})^2}{2(\alpha_e^2+\alpha_h^2)}\right] \times\frac{1}{2}\left[\mathrm{erf}\left(\frac{L\sqrt{p}}{2}+\frac{q}{\sqrt{p}}\right)+\mathrm{erf}\left(\frac{L\sqrt{p}}{2}-\frac{q}{\sqrt{p}}\right)\right], \quad \text{(A2)}$$

$$\langle\Psi_{10}\rangle_\infty = \frac{\alpha_e}{p}\left(\frac{q}{\sqrt{p}} + z_{0e}\sqrt{p}\right)\sqrt{\frac{\alpha_e\alpha_h}{2}} \times \exp\left[-\frac{\alpha_e^2\alpha_h^2(z_{0e}+z_{0h})^2}{2(\alpha_e^2+\alpha_h^2)}\right], \tag{A3}$$

$$\langle\Psi_{01}\rangle_\infty = \frac{\alpha_h}{p}\left(\frac{q}{\sqrt{p}} - z_{0h}\sqrt{p}\right)\sqrt{\frac{\alpha_e\alpha_h}{2}} \times \exp\left[-\frac{\alpha_e^2\alpha_h^2(z_{0e}+z_{0h})^2}{2(\alpha_e^2+\alpha_h^2)}\right], \tag{A4}$$

$$\langle\Psi_{10}\rangle_L = \frac{\alpha_e}{\sqrt{\pi}}\sqrt{\frac{\alpha_e\alpha_h}{2}}\exp\left[-\frac{\alpha_e^2\alpha_h^2(z_{0e}+z_{0h})^2}{2(\alpha_e^2+\alpha_h^2)}\right] \times \frac{1}{2p}\left\{\exp\left[-\left(\frac{L\sqrt{p}}{2}+\frac{q}{\sqrt{p}}\right)^2\right] - \exp\left[\left(\frac{L\sqrt{p}}{2}-\frac{q}{\sqrt{p}}\right)^2\right] + \left(\frac{q}{\sqrt{p}}+z_{0e}\sqrt{p}\right)\sqrt{\pi}\left[\mathrm{erf}\left(\frac{L\sqrt{p}}{2}+\frac{q}{\sqrt{p}}\right) + \mathrm{erf}\left(\frac{L\sqrt{p}}{2}-\frac{q}{\sqrt{p}}\right)\right]\right\}. \tag{A5}$$

and

$$\begin{aligned}\langle\Psi_{01}\rangle_L &= \langle e0|h1\rangle \\ &= \frac{\alpha_h}{\sqrt{\pi}}\sqrt{\frac{\alpha_e\alpha_h}{2}}\exp\left[-\frac{\alpha_e^2\alpha_h^2(z_{0e}+z_{0h})^2}{2(\alpha_e^2+\alpha_h^2)}\right] \\ &\times \frac{1}{2p}\left\{\exp\left[-\left(\frac{L\sqrt{p}}{2}+\frac{q}{\sqrt{p}}\right)^2\right] - \exp\left[\left(\frac{L\sqrt{p}}{2}-\frac{q}{\sqrt{p}}\right)^2\right] + \left(\frac{q}{\sqrt{p}}-z_{0h}\sqrt{p}\right)\sqrt{\pi} \times \left[\mathrm{erf}\left(\frac{L\sqrt{p}}{2}+\frac{q}{\sqrt{p}}\right) + \mathrm{erf}\left(\frac{L\sqrt{p}}{2}-\frac{q}{\sqrt{p}}\right)\right]\right\},\end{aligned} \tag{A6}$$

where erf( ) is the error function [19]. The quantities p and q are defined as

$$p = \tfrac{1}{2}\left(\alpha_e^2+\alpha_h^2\right), \qquad q = \tfrac{1}{2}\left(\alpha_h^2 z_{0h} - \alpha_e^2 z_{0e}\right). \tag{A7}$$

In all the above expressions, due to Eq. (18), one has to set $\alpha_e = \alpha_h$.

[1] M. Aßmann and M. Bayer, Adv. Quantum Technol. **2020**, 1900134 (2020).
[2] T. Kazimierczuk, D. Fröhlich, S. Scheel, H. Stolz, and M. Bayer, Nature (London) **514**, 344 (2014).
[3] M. Khazali, K. Heshami, and C. Simon, J. Phys. B **50**, 215301 (2017).
[4] V. Walther, R. Johne, and T. Pohl, Nat. Commun. **9**, 1309 (2018).
[5] D. Ziemkiewicz and S. Zielińska-Raczyńska, Opt. Lett. **43**, 3742 (2018).
[6] S. Zielińska-Raczyńska, G. Czajkowski, K. Karpiński, and D. Ziemkiewicz, Phys. Rev. B **99**, 245206 (2019).
[7] S. Zielińska-Raczyńska, D. Ziemkiewicz, and G. Czajkowski, Phys. Rev. B **94**, 045205 (2016).
[8] J. Heckötter, M. Freitag, D. Fröhlich, M. Aßmann, M. Bayer, M. A. Semina, and M. M. Glazov, Phys. Rev. B **95**, 035210 (2017).
[9] S. Stainhauer, M. A. Versteegh, S. Gyger, A. W. Elshaari, B. Kunert, A. Mysyrowicz, and V. Zwiller, Commun. Mater. **1**, 11 (2020).
[10] N. Naka, I. Akimoto, M. Shirai, and K. Kanno, Phys. Rev. B **85**, 035209 (2012).
[11] M. Takahata, K. Tanaka, and N. Naka, Phys. Rev. B **97**, 205305 (2018).
[12] S. A. Lynch, Ch. Hodges, S. Mandal, W. Langbein, R. P. Singh, L. A. P. Gallagher, J. D. Pritchett, D. Pizzey, J. P. Rogers, Ch. S. Adams, and M. P. A. Jones, *2018 20th International Conference on Transparent Optical Networks (ICTON), 2018*, pp. 1–4.
[13] K. Orfanakis, S. K. Rajendran, H. Ohadi, S. Zielińska-Raczyńska, G. Czajkowski, K. Karpiński, and D. Ziemkiewicz, Phys. Rev. B **103**, 245426 (2021).
[14] A. Konzelmann, B. Frank, and H. Giessen, J. Phys. B **53**, 024001 (2020).
[15] D. Ziemkiewicz, K. Karpiński, G. Czajkowski, and S. Zielińska-Raczyńska, Phys. Rev. B **101**, 205202 (2020).
[16] D. Ziemkiewicz, G. Czajkowski, K. Karpiński, and S. Zielińska-Raczyńska, Phys. Rev. B **103**, 035305 (2021).
[17] Y. H. Kuo, Y. Lee, Y. Ge, S. R. Jonathan, E. Roth, T. I. Kamins, D. A., B. Miller, and J. S. Harris, Nature (London) **437**, 1334 (2005).
[18] J. Heckötter, D. Fröhlich, M. Aßmann, and M. Bayer, Phys. Solid State **60**, 1595 (2018).
[19] M. Abramowitz and I. Stegun, *Handbook of Mathematical Functions* (Dover Publications, New York, 1965).
[20] S. Artyukhin, D. Fishman, C. Faugeras, M. Potemski, A. Revcolevschi, M. Mostovoy, and P. H. M. van Loosdrecht, Sci. Rep. **8**, 7818 (2018).
[21] D. Ziemkiewicz, G. Czajkowski, K. Karpiński, and S. Zielińska-Raczyńska, Phys. Rev. B **104**, 075304 (2021).
[22] P. Zielinski, P. Rommel, F. Schweiner, and J. Main, J. Phys. B: At. Mol. Opt. Phys. **53**, 054004 (2020).
[23] J. Heckötter, M. Freitag, D. Fröhlich, M. Aßmann, M. Bayer, M. A. Semina, and M. M. Glazov, Phys. Rev. B **98**, 035150 (2018).
[24] V. T. Agekyan, Phys. Status Solidi A **43**, 11 (1977).